⌘ *Author's Choice*

THE JOURNAL OF BIOLOGICAL CHEMISTRY VOL. 287, NO. 4, pp. 2759–2765, January 20, 2012

Cellulases Dig Deep

IN SITU OBSERVATION OF THE MESOSCOPIC STRUCTURAL DYNAMICS OF ENZYMATIC CELLULOSE DEGRADATION[*S]

Received for publication, May 4, 2011, and in revised form, November 25, 2011 Published, JBC Papers in Press, November 29, 2011, DOI 10.1074/jbc.M111.257717

Patricia Bubner[‡], Judith Dohr[§], Harald Plank[§], Claudia Mayrhofer[§], and Bernd Nidetzky[‡1]

From the [‡]Institute of Biotechnology and Biochemical Engineering, Graz University of Technology, Petersgasse 12, A-8010 Graz, Austria and the [§]Institute for Electron Microscopy, Graz University of Technology, Steyrergasse 17, A-8010 Graz, Austria

Background: The exact mechanism by which cellulases degrade cellulose is still elusive.
Results: An empirical model of the structural dynamics of cellulose degradation is shown.
Conclusion: Enzymatic cellulose hydrolysis is subjected to deceleration and acceleration caused by periodically emerging internal limitations and overcoming them.
Significance: Understanding structural dynamics of enzymatic cellulose disintegration is pivotal for making biofuel production from lignocellulosic feedstock economic.

Enzymatic hydrolysis of cellulose is key for the production of second generation biofuels, which represent a long-standing leading area in the field of sustainable energy. Despite the wealth of knowledge about cellulase structure and function, the elusive mechanism by which these enzymes disintegrate the complex structure of their insoluble substrate, which is the gist of cellulose saccharification, is still unclear. We herein present a time-resolved structural characterization of the action of cellulases on a nano-flat cellulose preparation, which enabled us to overcome previous limitations, using atomic force microscopy (AFM). As a first step in substrate disintegration, elongated fissures emerge which develop into coniform cracks as disintegration continues. Detailed data analysis allowed tracing the surface evolution back to the dynamics of crack morphology. This, in turn, reflects the interplay between surface degradation inside and outside of the crack. We observed how small cracks evolved and initially increased in size. At a certain point, the crack diameter stagnated and then started decreasing again. Stagnation corresponds with a decrease in the total amount of surface which is fissured and thus leads to the conclusion that the surface hydrolysis "around" the cracks is proceeding more rapidly than inside the cracks. The mesoscopic view presented here is in good agreement with various mechanistic proposals from the past and allows a novel insight into the structural dynamics occurring on the cellulosic substrate through cellulase action.

Long-term global efforts in the field of renewable energy aim at efficient utilization of lignocellulosic biomass for fuel production with the saccharification of cellulose being considered as the key bottleneck (1–5). In today's markets, a competitive commercial process requires the formation of soluble sugars from plant cell wall microfibrils being highly efficient. This efficiency, however, is largely restrained by what is referred to as substrate recalcitrance: the structural resistance of the insoluble cellulose core to enzymatic conversion manifesting itself in sluggish rates of hydrolytic breakdown of cellulose, even at high enzyme concentrations (1, 3). Overcoming cellulose recalcitrance, therefore, constitutes a central aim in biofuel development. Despite extensive research spanning over more than four decades, processes for cellulose hydrolysis are still advanced empirically because of insufficient understanding of the mechanisms underlying insoluble substrate deconstruction by enzyme action. Translating the wealth of knowledge about the structure and the catalytic function of cellulose-degrading enzymes (6; see CAZy the carbohydrate-active enzyme database) into comprehension of cellulase activity on the insoluble substrate has proven to be remarkably difficult, essentially because of two main complexities: first, the heterogeneous morphology of the cellulosic substrate (3); and second, the methodological difficulties in visualizing the action of cellulases on the cellulose surface at the nanometer scale (7–8). Schematic views of enzymatic hydrolysis of cellulose published nowadays have hence changed little compared with decades ago (4, 7, 9–10), which is the best evidence of the tedious progress made in the field. Multiple factors concerning the enzyme (*i.e.* mode of adsorption to substrate, individual components of cellulase systems showing synergy (cooperative interaction), product inhibition, stability) and the cellulosic substrate (*i.e.* crystallinity, available surface area, pore size, degree of polymerization) certainly play a crucial role in hydrolysis (9). The relative importance and interdependence of these factors will nevertheless remain elusive, pending clarification of fundamental questions.

In this article, we present a study employing atomic force microscopy (AFM)[2] in which we achieved a time-resolved *in situ* visualization of the effect of enzyme action on the surface of

* This work was supported by Grant P 24156-B21 from the Austrian Science Fund FWF (to B. N.).
⌘ *Author's Choice*—Final version full access.
[S] This article contains supplemental Figs. S1–S6 and Table S1.
[1] To whom correspondence should be addressed: Institute of Biotechnology and Biochemical Engineering, Graz University of Technology, Petersgasse 12, A-8010 Graz, Austria. Tel.: 43-316-873-8400; Fax: 43-316-873-8434; E-mail: bernd.nidetzky@tugraz.at.

[2] The abbreviations used are: AFM, atomic force microscopy; BMIMCl, 1-butyl-3-methylimidazolium chloride; CBH, cellobiohydrolase; DSC, differential scanning calorimetry; EDX, energy dispersive X-ray spectroscopy; EG, endoglucanase; FPU, filter paper unit; MS, mass spectrometry; RMS, root-mean-squared; TGA, thermogravimetric analysis; STA, simultaneous thermal analysis; XRD, X-ray diffraction.

cellulose at a nanoscale resolution. By using a special nano-flat preparation of cellulose we were able to directly monitor the complete process of deconstruction of the substrate from early fissuring events on the cellulose surface to the progressing surface erosion at longer hydrolysis times. We extracted the dynamic alteration of the cellulose surface structure quantitatively from AFM data, which reflects the interplay between surface degradation inside and outside of cracks. The cracks probably develop as a result of the combined laterally processive and penetrating actions of the adsorbed cellulases. This mesoscopic structural view on cellulose degradation provides a visualization of the dynamics occurring on the substrate during enzymatic cellulase degradation. Based on our results we suggest factors, which possibly are responsible for the peculiar crack characteristics observed (4, 9, 11–12).

EXPERIMENTAL PROCEDURES

Materials—All materials were purchased of the highest purity available from Carl Roth (Karlsruhe, Germany) unless stated otherwise. Avicel PH-101 and the glucose assay reagent were from Sigma-Aldrich. β-Glucosidase was from Novozymes (Bagsvaerd, Denmark).

Preparation of the Complete Cellulase System—We produced the complete cellulase system of *Trichoderma reesei* SVG 17 as described by Esterbauer *et al.* (13), supplemented it with 0.05% sodium azide, and stored it at 4 °C for the time course of the experiments. Routinely, we checked activity and protein content of the preparation to verify stability and consistency. As recommended by the IUPAC, we determined the cellulolytic activity using the well-established filter paper unit (FPU) assay (13–14). According to this assay, the cellulase system had a specific activity of 2.14 FPU/mg at a protein concentration of 0.5 mg/ml. We measured the protein concentration as described by Bradford (15) employing Roti®-Quant and Roti®-Nanoquant assays standardized with bovine serum albumin. For the preparation of appropriate dilutions and for the washing steps for the AFM experiments described below, we used a 50 mM sodium citrate buffer (pH 5.0), which is denoted as buffer.

Cellulose Substrate and Specimen Preparation—First, we prepared a primary cellulose gel according to a previously published protocol (16). Second, we cut the formed primary gel into small squares and removed the solvent and loosely bound water using a fractionated ethanol extraction step (stepwise from 30% to absolute ethanol). Subsequently the substrate was air-dried. This procedure resulted in a dehydrated gel. In contrast to the primary gel material, the dehydrated gel was stiff, non-transparent, and substantially smaller.

We performed x-ray diffraction (XRD) analysis of dehydrated gel samples using a Siemens D501 diffractometer (CuKα 1 radiation; Siemens, Munich, Germany). Additionally, we conducted combined differential scanning calorimetry (DSC)/thermogravimetric analysis (TGA) measurements with a Netzsch STA 449C (Netzsch Gerätebau GmbH, Selb, Germany) using a heat rate of 10 °C/min under a constant flow of helium (50.0 ml min^{-1}). We analyzed the gas products, which evolved in the course of the measurement online with a Netzsch QMS 403C quadrupole mass spectrometer.

To generate a stationary substrate for AFM investigation, we embedded the dehydrated gel in epoxy resin (supplemental Fig. S1) without employing elevated temperatures or pressure. We confirmed the absence of epoxy diffusion into the substrate experimentally by energy dispersive x-ray spectroscopy (EDX) measurements in a variable pressure scanning electron microscope (VP-S.E. Quanta 200 and Quanta 600). Finally, to achieve a nano-flat surface, the embedded specimen was subjected to ultramicrotomy using an Ultracut UCT (Leica microsystems, Wetzlar, Germany).

Experimental Strategy, and AFM Data Collection—Prior to cellulase exposure, we recorded AFM reference images of the dry substrate at defined areas. Thereafter, we allowed the substrate to equilibrate in buffer at room temperature for 2 h. Again, we recorded AFM reference images at defined areas. Following this, we incubated the substrate in the complete cellulase system at an appropriate dilution to achieve the desired enzyme/substrate ratio (36; 3.6; 0.36 $mg/g_{substrate}$) for the time indicated below at 30 °C without agitation. Then, we performed appropriate AFM control measurements of the substrate samples incubated at 30 °C in buffer continuously (supplemental Fig. S2). This was done to affirm the absence of surface alteration by buffer alone or by the applied washing and blow-drying process performed before AFM imaging as described below.

After each incubation step during the discontinuous strategy, we withdrew the substrate from the enzyme solution, washed it three times in buffer, blow-dried by CO_2 spraying, measured it using the AFM, and afterward re-incubated it in a fresh enzyme dilution at the breakpoints indicated as follows (referring to total incubation time): 30 min, 60 min, 90 min (36 $mg_{protein}/g_{substrate}$); 15 min, 45 min, 105 min, 165 min, 225 min, 285 min (3.6 $mg_{protein}/g_{substrate}$); 30 min; 90 min; 210 min; 450 min (0.36 $mg_{protein}/g_{substrate}$). For continuous measurements, the incubation time was 90 min for 36 $mg_{protein}/g_{substrate}$; 285 min for 3.6 $mg_{protein}/g_{substrate}$; and 450 min for 0.36 $mg_{protein}/g_{substrate}$, respectively. Eventually, we dried these samples as described above for the discontinuous samples.

We used a commercial Dimension 3100 AFM equipped with a Hybrid scanner and Nanoscope IVa controller (Bruker AXS, Santa Barbara) for all AFM measurements. We performed the imaging in tapping mode on dry substrate surfaces in air with an OMCL-AC 240/160 TS silicon probe (Olympus, Tokyo, Japan). To guarantee relevance and comparability of individual measurements, images were always obtained at identical areas using the same scan sizes. We chose the scan rates, setpoints and drive amplitudes appropriately to obtain stable scanning with the lowest energy dissipation possible. During image recording, we gave careful consideration to avoiding tip-related artifacts by permanently evaluating sidewall angles and morphological features of the surface.

AFM Image Analyses—We performed detailed image analysis using the software packages Research Nanoscope (V7.13, Bruker, AXS) and Gwyddion (V2.2) to quantify observed features and confirm extracted data by cross-checking the results. To prove non-monotonic development of cracks, it was essential to gain information about the geometry of selected individual cracks, *i.e.* length, width, and depth. To assure reliability, we

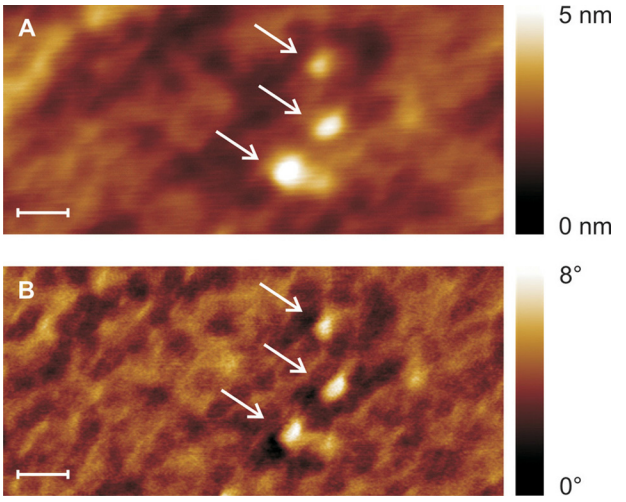

FIGURE 1. **Visualization of single cellulases in an emerging crack.** Height (*A*) and phase (*B*) image of a 200 nm scan, taken ~15 min after incubation with a cellulase concentration of 0.36 $mg_{protein}/g_{substrate}$, exhibit features not observed on the buffer-swollen image blank. These new features are ~5 nm in diameter and show a distinct phase signal (no slope effects). It is therefore very likely that they are single cellulases. The scale bar represents 20 nm.

thoroughly pre-investigated side walls of the cracks with respect to AFM tip-related limitations.

We extracted data describing the changing topology of the overall substrate surface, *i.e.* root-mean-squared (RMS) surface roughness, crack footprint, and number of cracks, with carefully adapted masking tools including height and curvature filters. To estimate the error of analyses, we did over- and underestimation of the applied masks on purpose, and we chose the maximum deviation as error. To follow the trend of the footprint over time, we compared the extracted footprint areas of identical sample areas with same scan size at specified points in time. Additionally, merging of cracks was proven both through observing the time-dependent evolution of cracks during enzymatic attack and by statistical methods. Finally, high resolution phase imaging, which yields the image of the dissipative interaction energy density, allowed for localization of enzymes on the substrate (Fig. 1).

Enzymatic Hydrolysis of Cellulose—We performed accompanying hydrolysis experiments and designed them to resemble the conditions used in the AFM experiments. To this end, we incubated samples of the dehydrated gel continuously or discontinuously at the three different enzyme loadings employed (36; 3.6; 0.36 $mg/g_{substrate}$) in buffer. The incubation time was the same as described above for discontinuous and continuous experiments. The samples were washed three times in buffer and dried in the same way as for AFM investigations.

Samples withdrawn at the respective breakpoints were boiled to stop the reaction, chilled on ice, and centrifuged (4 °C, 13,000 rpm, 10 min). Then, we added 1.2 units of β-glucosidase to the supernatant, incubated it at 50 °C for 30 min and stopped the reaction as described above. Eventually, the amount of glucose in the supernatant was determined using a glucose assay reagent according to the manufacturer's protocol.

RESULTS AND DISCUSSION

Specimen Preparation and Characterization—Not unexpectedly, the reproducible preparation of a cellulosic substrate specimen suitable for AFM analysis presented a critical challenge: to make a general statement about cellulose degradation, it is, first of all, crucial that the substrate is chemically unmodified. Second, studying cellulase attack by means of AFM requires a homogeneously smooth, nano-flat surface. In a recent AFM study, which aimed at understanding the mechanism of cellobiohydrolase (CBH) I an important finding was published: CBHI preferably attacks crystalline cellulose at the hydrophobic faces (2). The types of native and processed celluloses applied in earlier AFM studies, however, were limiting in various ways (2, 7, 17–20). The use of highly crystalline cellulose alone, for instance, does not allow the investigation of an entire cellulase system featuring CBHs and endoglucanases (EGs), with the latter ones being known to preferably attack amorphous areas (2, 9, 11, 18, 21). In contrast to previous research, we took a distinct approach involving the dissolution of the microcrystalline cellulose Avicel in the ionic liquid 1-butyl-3-methylimidazolium chloride (BMIMCl) at 100 °C, which, upon cooling, resulted in a gel-like material (16). From this primary gel material we then removed the ionic liquid and excess water using ethanol, which yielded a dehydrated gel of pure cellulose. We want to emphasize that this type of preparation does not involve precipitation of amorphous cellulose from the ionic liquid (22). It is rather a dissolution process involving formation of a gel consisting of BMIMCl, water, both loosely and tightly bound, and cellulose. Dehydration with ethanol removes a significant amount of water as well as all of the ionic liquid from this primary gel as confirmed by STA and MS analyses (Fig. 2, supplemental Table S1) (16, 23). Thus, the dehydrated gel is a pure cellulosic substrate. In accordance with Prasad *et al.* (16), evidence from XRD analysis revealed a predominantly amorphous substrate structure with, however, some regions of higher order (Fig. 3). The presence of a broad peak of low intensity in the XRD graph indicates that only a small amount of crystalline cellulose is present. These highly ordered areas are reflected in a major peak of crystalline cellulose I at θ-2θ 22.7° (24). Along with cellulose I, a minor fraction of cellulose II is also present (θ-2θ 19.8°) (24). Therefore, our substrate is a mixed crystalline-amorphous cellulose.

The RMS surface roughness of the dehydrated gel was 8–10 nm after a 2-h equilibration period in buffer. Compared with the size of the catalytic unit of a typical cellulase (~ 6 nm (25)), this clearly validates the above mentioned substrate for the purpose of this study in terms of surface smoothness. This special preparation enabled us not only to localize single enzymes *in situ* (Fig. 1), but also to observe the dynamic change of the surface during hydrolysis (9, 11).

AFM Investigation of Enzymatic Cellulose Disintegration—For the examination of substrate degradation we employed the cellulolytic enzyme system of the soft-rot fungus *T. reesei* (9, 13). This well-known cellulase contains all the individual activities required for an efficient breakdown of crystalline cellulose into soluble sugars, including CBHs, which cleave cellulose chains from the chain end ("exo"), and EGs, which cleave in the middle of a chain ("endo"). As the first step in our study, we incubated the cellulose specimen at 30 °C in sodium citrate buffer containing a defined amount of cellulose, which we varied at three different levels reflecting limiting, intermediate, and saturating

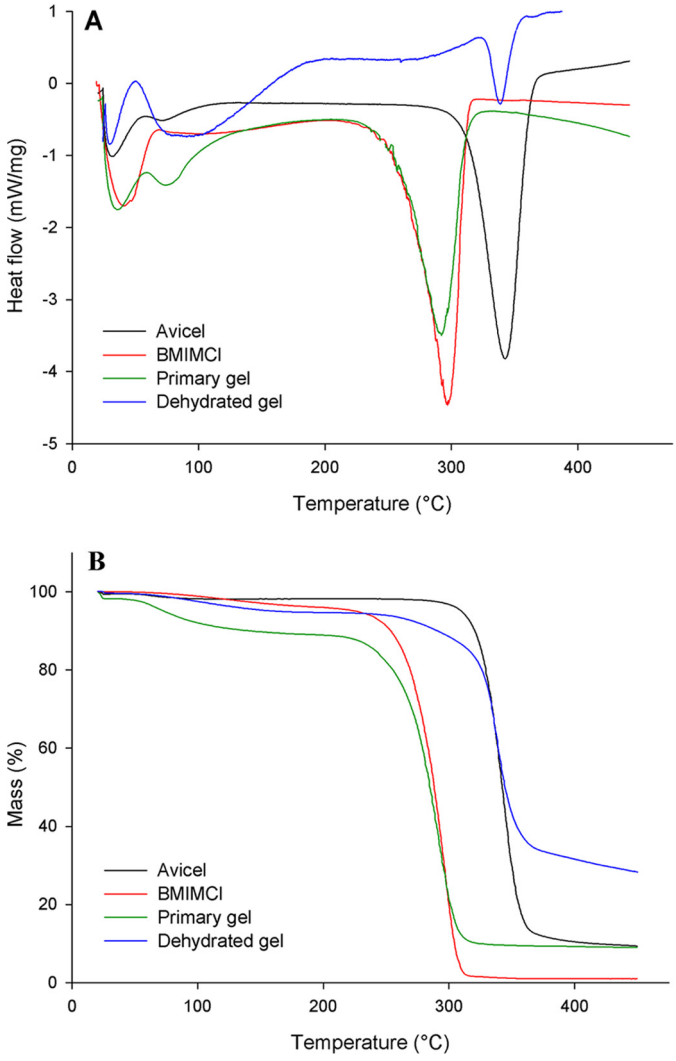

FIGURE 2. **STA curves of microcrystalline cellulose (Avicel), the ionic liquid BMIMCl, the primary and the dehydrated gel.** DSC (*A*) and TGA (*B*) measurements show remarkable differences in behavior of the dehydrated gel as compared with the primary gel. In both graphs the behavior of the dehydrated gel sample more closely resembles the one of the microcrystalline cellulose than the one of the primary gel. *B*, the difference in weight loss at 100 °C indicates a pronounced loss of water in the primary gel but not in the dehydrated gel.

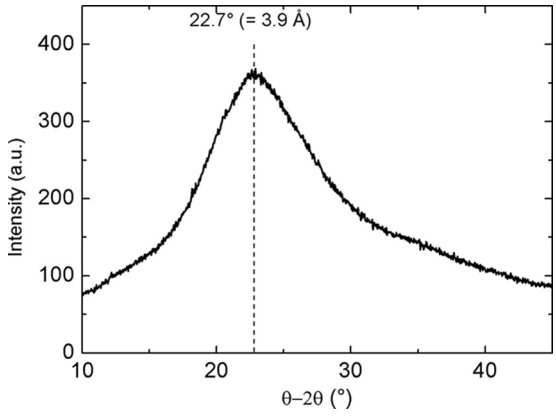

FIGURE 3. **XRD profile of a dehydrated cellulose gel sample.** The main peak at 22.7°, which corresponds to crystalline cellulose I, is *highlighted*.

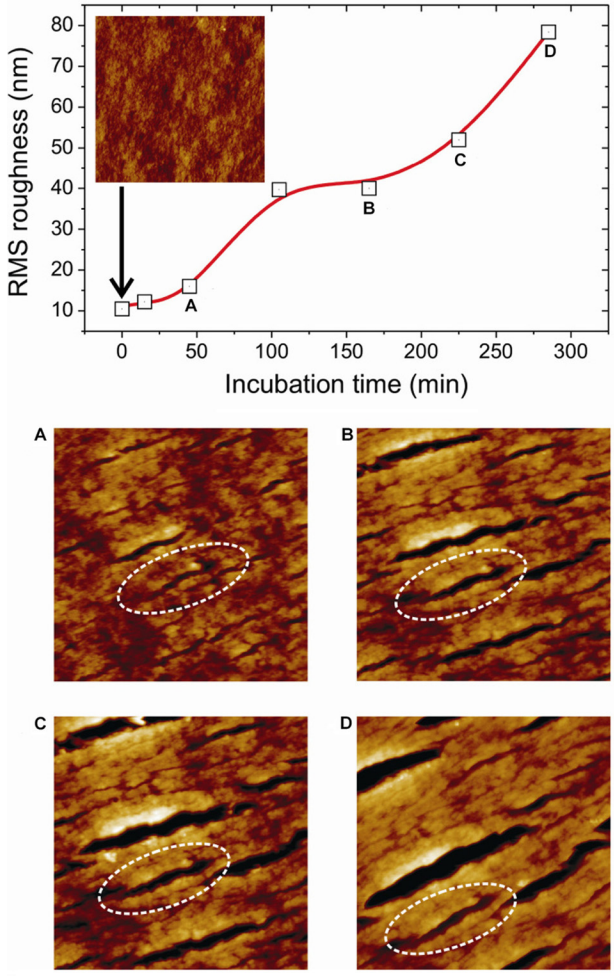

FIGURE 4. **Enzymatic cellulose degradation reflected by RMS roughness variation.** The image at 0 min shows the nano-flat surface after buffer swelling. Images *A* to *D* reveal the formation of elongated cracks with time at a cellulase loading of 3.6 $mg_{protein}/g_{substrate}$. As an example, a representative crack is *circled*, and it is shown how it grows at first (*A* and *B*), then stagnates (*C* compared with *B*), and eventually becomes narrower (*D* compared with *C*).

adsorption of enzyme on the cellulose surface (36; 3.6; 0.36 $mg_{protein}/g_{substrate}$). At certain breakpoints, we interrupted the enzyme action by removing the substrate, which we subsequently washed by dipping into buffer. Upon blow-drying, we performed AFM imaging. Thereafter, we placed the sample into a fresh enzyme solution with the same cellulase concentration as before and incubated it until the next breakpoint. To rule out that the effects observed are biased by washing and re-incubation, we analyzed controls subjected to continuous incubation. The comprehensive data set thus obtained allows for quantitative monitoring of the disintegration of the cellulose surface upon enzymatic attack (Fig. 4). In this article, we discuss the results measured at intermediate enzyme loading as they gave the best resolution with respect to incubation time. At extended incubation times and/or higher enzyme loading, tip limitations occurred as a result of the deeply rugged surface. The overall pattern of surface disruption, however, was independent of the amount of enzyme applied (supplemental Fig. S3).

Visualization Results and Implications—Intriguingly, the first snapshot of the enzymatic reaction (Fig. 4*A*) shows elon-

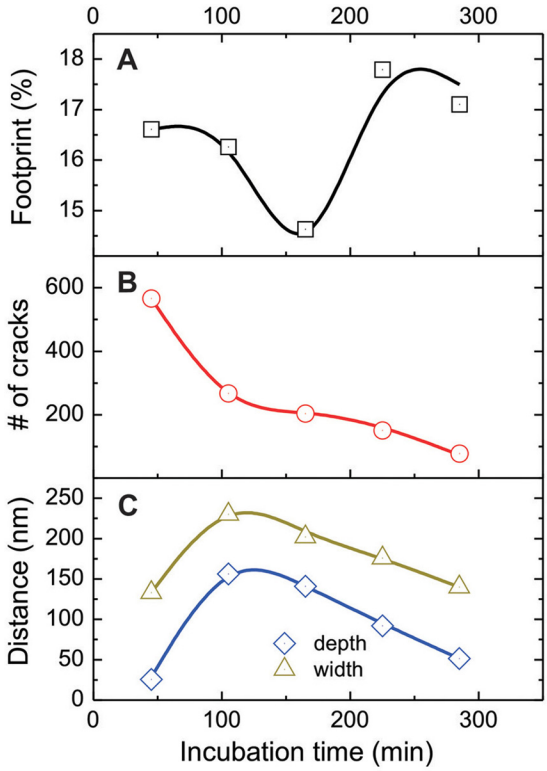

FIGURE 5. **Quantitative analysis of AFM data.** *A*, course of the crack footprint over time. *B*, the total number of cracks is decreasing over time, despite constantly emerging new cracks. This is a result of numerous merging events, which eventually lead to a network of valleys on the substrate surface. *C*, development of depth and width of a representative small crack.

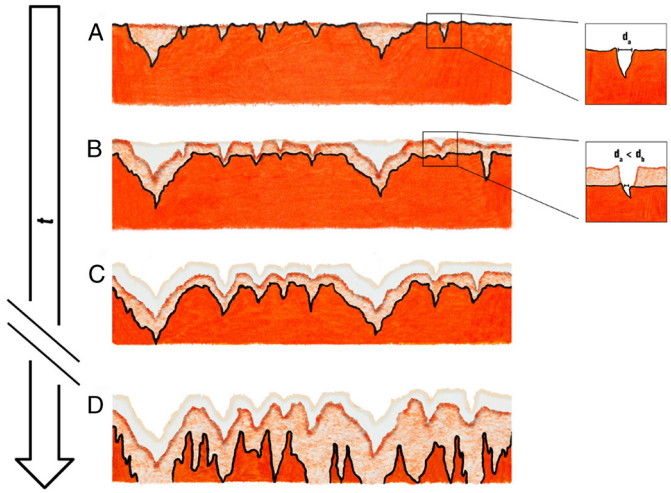

FIGURE 6. **Model of enzymatic cellulose digestion based on quantitative AFM data.** This schematic model aims at visualizing the mesoscopic perspective on enzymatic disruption of cellulose. Along the timeline we follow the cellulolytic degradation of the surface from random early fissuring events (*A*) to a completely fissured surface, where the entire external surface has been consumed and rate retarding factors become operative (*D*). The proportions in *A* through *C* reflect typical dimensions observed in relevant AFM measurements.

gated fissures, which have instantly emerged all over the surface. They are aligned in their elongation direction, implying a preferred direction of enzymatic processing on the surface. This finding correlates well with the observation of processive action of CBHI, which was confirmed by AFM in recent publications (2, 7). Cellulose surface fissuring was mirrored in an increase of overall RMS roughness. Interestingly, however, RMS roughness did not evolve continuously but rather stepwise, passing through a distinct plateau of constant RMS roughness (Fig. 4). Considering the small experimental error of ±1.5 nm, the data points strongly suggest the presence of this plateau. Furthermore, we observed the appearance of an RMS roughness plateau at all three cellulase concentrations studied (36; 3.6; 0.36 $mg_{protein}/g_{substrate}$) (supplemental Fig. S4). For the two higher loadings, AFM measurements are not reliable at extended incubation times because of AFM tip limitations. These are caused by deep cracks formed during longer incubation times.

Detailed analysis of the time dependence of the crack footprint gave further insight into the peculiar dynamics of RMS surface roughness: this footprint is a measure of the percentage of substrate surface that has become fissured by enzymatic attack. Strikingly, the RMS roughness reaching its plateau coincided with the decrease of the crack footprint, passing through its minimum value at the end of the plateau phase. Then the course of the crack footprint rises to a temporary maximum (Fig. 5*A*). Already fissured surface can obviously not be rebuilt in the enzymatic process; the observed decrease in crack footprint therefore inevitably implies that diminution in the cross-section of the formed cracks must occur. In fact, this is solely explained through advancing degradation of the surface outside the crack taking the lead over intra-crack hydrolysis, thereby causing an overall surface reduction (Fig. 6). The question now is, why is surface degradation ("external rate") proceeding continuously whereas hydrolysis in the small cracks ("internal rate") is stalled? Generally, appearance of internal rate limitation seems to be local and temporary until the limiting factors supposedly are neutralized by external hydrolysis promoting cross-section diminution and crack merging. The discontinuation of the internal rate limitation is clearly indicated by the increase in the crack footprint at longer reaction times. This signifies a further increase in cracked surface, which was not reflected by an increasing total number of cracks, indicating the occurrence of merging events (Fig. 5*B*).

In Fig. 5*C*, we selected a typical small crack and extracted data about the evolution of its width and depth over time. Both parameters increased steeply at first, reaching their maximum at 105 min. Subsequently, width and depth decreased, thus causing a cross-section diminution as indicated by the crack footprint. Unexpectedly, this occurred despite a simultaneously increasing overall RMS roughness (Fig. 4). These opposed trends of development of crack size parameters and RMS roughness can only be accounted for by an overall surface reduction, well consistent however, with the observation of a concurrent increase in the crack footprint (Fig. 5*A*). If smallish cracks lose rather than gain in size, the observed increase in RMS roughness must be due to three major reasons: first, constantly evolving new fissures; second, concomitant elongation of existing small and medium cracks; and finally, constant overall growth of the large cracks in both width and length. Concerning the latter one, the decrease in crack number over time (Fig. 5*B*) indicates that crack coalescence is partially involved in the growth of these cracks. Fig. 4 shows the time course of RMS

roughness supported by AFM images. These images reveal the dynamics of the cross-sectional area of a rather small crack alongside the unrestrained growth of a large crack. RMS roughness would seem to pass through the observed plateau at the point where hydrolysis in small cracks becomes limiting overall ("deceleration"), only to increase when surface hydrolysis has overcome the internal limitations ("acceleration").

The causes for the internal rate deceleration in small cracks could be substrate-related as well as enzyme-related. Concerning the substrate, cracks might be the result of a primary attack on cellulose regions of lower order. Consequently, hydrolysis would slow down when this material is digested, leaving regions of higher order behind which are harder to degrade. With regard to the enzymes, diffusional restrictions occurring in the confined space of the cracks might influence cellulolytic activity at two different levels: first, through loss of synergy among individual cellulase components and second, by product inhibition.

According to the literature (26), the maximum accessible radius of a cylindrical pore with a diameter of 3 nm is 1.31 nm, which illustrates how the space in narrowing pores becomes limiting for macromolecules. On top of that, wall confinement plays an increasingly important role when the diffusing molecule is ten times or less smaller than the diameter of the pore. For example, for a cylindrical pore with a diameter of 1.5 nm, which is about five times the size of a water molecule, the axial diffusion coefficient for water was calculated to be 3.43×10^{-5} cm^2/s as compared with in bulk (5.19×10^{-5} cm^2/s) (26). In case of a typical cellulase with its ellipsoid core shape having a diameter of 4–6.5 nm and a total enzyme length of 18–21.5 nm (25, 27, 29), this implies that every pore having a so called critical width of about 40–60 nm will already limit macromolecule diffusion to a high degree by wall confinement. Probably, even bigger pores up to 200 nm limit diffusion to a certain extent, especially, when previously bound enzymes add up to the confinement effect. Thus, dynamic features of cellulase adsorption to cellulose, in particular the exchange of complementary endo- and exo-enzyme activities on the substrate surface, might become attenuated within narrow cracks.[3] Furthermore, a possible sliding movement of exo-acting enzymes could be hampered. The basis for synergistic interaction between cellulases would thus be gradually removed, and deactivation of enzymes and pore clogging by protein aggregates might receive significance through phenomena such as irreversible adsorption, jamming, and aggregation (9–11, 30–31).

As a known fact, cellobiose is the main product of cellulose hydrolysis and strongly inhibits CBHI, the major protein component and "pacemaker" exo-enzyme of the *T. reesei* cellulase system (12). According to the dynamics we observed, we think it is conceivable that the formation of a concentration gradient for cellobiose might be promoted by restricted diffusivity within narrow cracks. This would *a fortiori* be favored by partial size exclusion of β-glucosidase by confinement effects discussed above. β-Glucosidase is a natural companion enzyme of the actual cellulases. This enzyme, which lacks the ability to adsorb to cellulose, cleaves cellobiose to yield glucose. As a matter of fact, the cellobiose binding constant of the *T. reesei* cellulase system is greater by a factor of 6 than its glucose binding constant, which makes glucose considerably less inhibitory than cellobiose (9, 32). Actually, when comparing our continuous and discontinuous AFM experiments, we found that continuous hydrolysis results in essentially the same surface disruptions but proceeds much more slowly than discontinuous hydrolysis (supplemental Fig. S5). The discontinuous setup involved repeated removal of the supernatant, thus probably alleviating high local product concentrations. It should therefore be interesting to perform in the future a quantitative analysis of diffusional restrictions of the cellulase activity, using the geometrical features of the formed cracks as an essential basis.

An Empirical Model of Enzymatic Cellulose Disintegration—The mesoscopic view of enzymatic disintegration of cellulose presented here sheds new light on what was hitherto known about the mechanism of cellulose disruption. The overall surface disruption caused by cellulase action is not a mere surface phenomenon or proceeds layer-wise (28): by contrast, it seems to consist of an external (*surface erosion*) and internal (*surface penetration*) component. As visualized in Fig. 6, the evolution of surface structural features along the reaction timeline are proposed to reflect the dynamics of surface erosion and penetration rates: in the initial phase of hydrolysis, the reaction would proceed "acceleratedly" (Fig. 6*A*). Then, the transient occurrence of internal limitations would lead to a "deceleration", meaning that surface hydrolysis predominates, thus causing cross-section diminution of those cracks where limiting factors prevail (Fig. 6*B*). As soon as these limitations are overcome by the ever progressing surface erosion, acceleration would occur again (Fig. 6, *B* and *C*).

We want to emphasize that, because of tip limitations, our study captures only the early phase of hydrolysis where the rate proceeds linearly (supplemental Fig. S6). Hence, our observations cover the early stage processes, which exhibit deceleration and acceleration caused by periodically emerging internal limitations and overcoming them. Presuming that this stage is the basis of the entire hydrolysis process, the observed processes in this phase are extremely interesting. Phenomena occurring at this point are likely to recur or possibly even to continue periodically throughout hydrolysis. Figuring that the observed early-phase processes persist through the entire course of cellulose saccharification, this might provide an explanation for the pronounced rate limitation, which was observed with essentially all types of cellulosic substrates. This typically occurs at 20–40% of conversion of the solid material (30–31). According to our suggested model, the substrate surface will be completely rugged at some point, far ahead of what we are able to observe using AFM, with essentially the entire external surface area consumed (Fig. 6*D*). At this point, internal limitations will prevail and acceleration will be stalled completely, thus causing a decline in soluble sugar formation. This, in turn, is reflected in the stagnation of the hydrolysis rate.

The model we developed based on the observations and quantitative evaluation of our AFM studies connects and provides a possible explanation for the different "rate-retarding factors," which have been proposed in literature before: inhibition by cellobiose, (apparent) enzyme deactivation, loss of syn-

[3] Note: the dynamics of cellulase adsorption and desorption were not followed in the course of the AFM measurements.

ergism, and decrease of substrate reactivity. Our visualization also implies that these factors are causative related to each other, and our model serves to expand the knowledge gained about early stage processes on the entire hydrolysis process.

Acknowledgments—We thank Karin Longus for producing the complete cellulase system; Nadejda Matsko for assistance in substrate preparation; Gregor Trimmel and Thomas Haber for characterization of the substrate; Joachim Krenn and Ferdinand Hofer for helpful discussions; and Dominika Stiger for carefully reading the manuscript. Special thanks go to Monika Hitter who contributed the professional artwork for the model of cellulose degradation (Fig. 6). B.N. acknowledges his involvement in the Austrian Centre of Industrial Biotechnology and the project "MacroFun - Bioengineering of Functional Macromolecules."

REFERENCES

1. Lynd, L. R., Laser, M. S., Bransby, D., Dale, B. E., Davison, B., Hamilton, R., Himmel, M., Keller, M., McMillan, J. D., Sheehan, J., and Wyman, C. E. (2008) How biotech can transform biofuels. *Nat. Biotechnol.* **26,** 169–172
2. Liu, Y. S., Baker, J. O., Zeng, Y., Himmel, M. E., Haas, T., and Ding, S. Y. (2011) Cellobiohydrolase hydrolyzes crystalline cellulose on hydrophobic faces. *J. Biol. Chem.* **286,** 11195–11201
3. Himmel, M. E., Ding, S. Y., Johnson, D. K., Adney, W. S., Nimlos, M. R., Brady, J. W., and Foust, T. D. (2007) Biomass recalcitrance: engineering plants and enzymes for biofuels production. *Science* **315,** 804–807
4. Arantes, V., and Saddler, J. N. (2010) Access to cellulose limits the efficiency of enzymatic hydrolysis: the role of amorphogenesis. *Biotechnol. Biofuels* **3,** 4
5. Solomon, B. D., Barnes, J. R., and Halvorsen, K. E. (2007) Grain and cellulosic ethanol: History, economics, and energy policy. *Biomass Bioenerg.* **31,** 416–425
6. Cantarel, B. L., Coutinho, P. M., Rancurel, C., Bernard, T., Lombard, V., and Henrissat, B. (2009) The Carbohydrate-Active EnZymes database (CAZy): an expert resource for Glycogenomics. *Nucleic Acids Res.* **37,** D233–238
7. Igarashi, K., Koivula, A., Wada, M., Kimura, S., Penttilä, M., and Samejima, M. (2009) High speed atomic force microscopy visualizes processive movement of *Trichoderma reesei* cellobiohydrolase I on crystalline cellulose. *J. Biol. Chem.* **284,** 36186–36190
8. Ding, S. Y., Xu, Q., Crowley, M., Zeng, Y., Nimlos, M., Lamed, R., Bayer, E. A., and Himmel, M. E. (2008) A biophysical perspective on the cellulosome: new opportunities for biomass conversion. *Curr. Opin. Biotechnol.* **19,** 218–227
9. Lynd, L. R., Weimer, P. J., van Zyl, W. H., and Pretorius, I. S. (2002) Microbial cellulose utilization: fundamentals and biotechnology. *Microbiol. Mol. Biol. Rev.* **66,** 506–577
10. Bansal, P., Hall, M., Realff, M. J., Lee, J. H., and Bommarius, A. S. (2009) Modeling cellulase kinetics on lignocellulosic substrates. *Biotechnol. Adv.* **27,** 833–848
11. Mansfield, S. D., Mooney, C., and Saddler, J. N. (1999) Substrate and enzyme characteristics that limit cellulose hydrolysis. *Biotechnol. Prog.* **15,** 804–816
12. Zhang, Y. H., and Lynd, L. R. (2004) Toward an aggregated understanding of enzymatic hydrolysis of cellulose: noncomplexed cellulase systems. *Biotechnol. Bioeng.* **88,** 797–824
13. Esterbauer, H., Steiner, W., Labudova, I., Hermann, A., and Hayn, M. (1991) Production of *Trichoderma* cellulase in laboratory and pilot scale. *Biores. Technol.* **36,** 51–65
14. Ghose, T. K. (1987) Measurement of cellulase activities. *Pure Appl. Chem.* **59,** 257–268
15. Bradford, M. M. (1976) A rapid and sensitive method for the quantitation of microgram quantities of protein utilizing the principle of protein-dye binding. *Anal. Biochem.* **72,** 248–254
16. Prasad, K., Kaneko, Y., and Kadokawa, J. (2009) Novel gelling systems of kappa-, iota-, and lambda-carrageenans and their composite gels with cellulose using ionic liquid. *Macromol. Biosci.* **9,** 376–382
17. Nigmatullin, R., Lovitt, R., Wright, C., Linder, M., Nakari-Setälä, T., and Gama, M. (2004) Atomic force microscopy study of cellulose surface interaction controlled by cellulose binding domains. *Colloids Surf. B Biointerfaces* **35,** 125–135
18. Lee, I., Evans, B. R., and Woodward, J. (2000) The mechanism of cellulase action on cotton fibers: evidence from atomic force microscopy. *Ultramicroscopy* **82,** 213–221
19. Quirk, A., Lipkowski, J., Vandenende, C., Cockburn, D., Clarke, A. J., Dutcher, J. R., and Roscoe, S. G. (2010) Direct visualization of the enzymatic digestion of a single fiber of native cellulose in an aqueous environment by atomic force microscopy. *Langmuir* **26,** 5007–5013
20. Liu, H., Fu, S., Zhu, J. Y., Li, H., and Zhan, H. (2009) Visualization of enzymatic hydrolysis of cellulose using AFM phase imaging. *Enzyme Microbrial Technol.* **45,** 274–281
21. Nieves, R. A., Ellis, R. P., Todd, R. J., Johnson, T. J., Grohmann, K., and Himmel, M. E. (1991) Visualization of *Trichoderma reesei* cellobiohydrolase I and endoglucanase I on aspen cellulose by using monoclonal antibody-colloidal gold conjugates. *Applied Environ. Microbiol.* **57,** 3163–3170
22. Zhao, H., Jones, C. L., Baker, G. A., Xia, S., Olubajo, O., and Person, V. N. (2009) Regenerating cellulose from ionic liquids for an accelerated enzymatic hydrolysis. *J. Biotechnol.* **139,** 47–54
23. Ohtani, H., Ishimura, S., and Kumai, M. (2008) Thermal decomposition behaviors of imidazolium-type ionic liquids studied by pyrolysis-gas chromatography. *Anal. Sci.* **24,** 1335–1340
24. Kim, S. J., Dwiatmoko, A. A., Choi, J. W., Suh, Y. W., Suh, D. J., and Oh, M. (2010) Cellulose pretreatment with 1-*n*-butyl-3-methylimidazolium chloride for solid acid-catalyzed hydrolysis. *Bioresour. Technol.* **101,** 8273–8279
25. Abuja, P. M., Schmuck, M., Pilz, I., Tomme, P., Claeyssens, M., and Esterbauer, H. (1988) Structural and functional domains of cellobiohydrolase I from *Trichodesma reesei*. *Eur. Biophys. J.* **15,** 339–342
26. Cui, S. T. (2005) Molecular self-diffusion in nanoscale cylindrical pores and classical Fick's Law predictions. *J. Chem. Phys.* **123,** 054706
27. Abuja, P. M., Pilz, I., Claeyssens, M., and Tomme, P. (1988) Domain structure of cellobiohydrolase II as studied by small angle X-ray scattering: close resemblance to cellobiohydrolase I. *Biochem. Biophys. Res. Commun.* **156,** 180–185
28. Penttilä, P. A., Várnai, A., Leppänen, K., Peura, M., Kallonen, A., Jääskeläinen, P., Lucenius, J., Ruokolainen, J., Siika-Aho, M., Viikari, L., and Serimaa, R. (2010) Changes in submicrometer structure of enzymatically hydrolyzed microcrystalline cellulose. *Biomacromolecules* **11,** 1111–1117
29. Kleywegt, G. J., Zou, J. Y., Divne, C., Davies, G. J., Sinning, I., Ståhlberg, J., Reinikainen, T., Srisodsuk, M., Teeri, T. T., and Jones, T. A. (1997) The crystal structure of the catalytic core domain of endoglucanase I from Trichoderma reesei at 3.6 A resolution, and a comparison with related enzymes. *J. Mol. Biol.* **272,** 383–397
30. Levine, S. E., Fox, J. M., Blanch, H. W., and Clark, D. S. (2010) A mechanistic model of the enzymatic hydrolysis of cellulose. *Biotechnol. Bioeng.* **107,** 37–51
31. Bommarius, A. S., Katona, A., Cheben, S. E., Patel, A. S., Ragauskas, A. J., Knudson, K., and Pu, Y. (2008) Cellulase kinetics as a function of cellulose pretreatment. *Metab. Eng.* **10,** 370–381
32. Holtzapple, M., Cognata, M., Shu, Y., and Hendrickson, C. (1990) Inhibition of *Trichoderma reesei* cellulase by sugars and solvents. *Biotechnol. Bioeng.* **36,** 275–287